Astronomy & Astrophysics

Tentative co-orbital submillimeter emission within the Lagrangian region L_5 of the protoplanet PDS 70 b

O. Balsalobre-Ruza[1] , I. de Gregorio-Monsalvo[2] , J. Lillo-Box[1] , N. Huélamo[1], Á. Ribas[3] ,
M. Benisty[4,5], J. Bae[6] , S. Facchini[7] , and R. Teague[8]

[1] Centro de Astrobiología (CAB), CSIC-INTA, Camino Bajo del Castillo s/n, 28692 Villanueva de la Cañada, Madrid, Spain
   e-mail: obalsalobre@cab.inta-csic.es
[2] European Southern Observatory, Alonso de Córdova 3107, Casilla 19, Vitacura, Santiago, Chile
[3] Institute of Astronomy, University of Cambridge, Madingley Road, Cambridge CB3 0HA, UK
[4] Laboratoire Lagrange, Université Côte d'Azur, CNRS, Observatoire de la Côte d'Azur, 06304 Nice, France
[5] Univ. Grenoble Alpes, CNRS, IPAG, 38000 Grenoble, France
[6] Department of Astronomy, University of Florida, Gainesville, FL 32611, USA
[7] Dipartimento di Fisica, Università degli Studi di Milano, Via Celoria 16, 20133 Milano, Italy
[8] Department of Earth, Atmospheric, and Planetary Sciences, Massachusetts Institute of Technology, Cambridge, MA 02139, USA

ABSTRACT

Context. High-spatial resolution Atacama Large Millimeter/submillimeter Array (ALMA) data have revealed a plethora of substructures in protoplanetary disks. Some of those features are thought to trace the formation of embedded planets. One example is the gas and dust that accumulated in the co-orbital Lagrangian regions L_4/L_5, which were tentatively detected in recent years and might be the pristine material for the formation of Trojan bodies.

Aims. This work is part of the TROY project, whose ultimate goal is to find robust evidence of exotrojan bodies and study their implications in the exoplanet field. Here, we focus on the early stages of the formation of these bodies by inspecting the iconic system PDS 70, the only confirmed planetary system in formation.

Methods. We reanalyzed archival high-angular resolution Band 7 ALMA observations from PDS 70 by doing an independent imaging process to look for emission in the Lagrangian regions of the two detected gas giant protoplanets, PDS 70 b and c. We then projected the orbital paths and visually inspected emission features at the regions around the L_4/L_5 locations as defined by ±60° in azimuth from the planet position.

Results. We found emission at a ∼4-σ level (∼6-σ when correcting from a cleaning effect) at the position of the L_5 region of PDS 70 b. This emission corresponds to a dust mass in a range of 0.03–2 M_{Moon}, which potentially accumulated in this gravitational well.

Conclusions. The tentative detection of the co-orbital dust trap that we report requires additional observations to be confirmed. We predict that we could detect the co-orbital motion of PDS 70 b and the dust presumably associated with L_5 by observing again with the same sensitivity and angular resolution as early as February 2026.

Key words. techniques: interferometric – planet-disk interactions – stars: early-type – planets and satellites: detection –
planets and satellites: formation – protoplanetary disks

1. Introduction

Trojan asteroids are common inhabitants of the Solar System. They are minor bodies[1] populating the L_4 and L_5 Lagrange regions of a planet, leading and trailing it 60° apart in the same orbital path. Laughlin & Chambers (2002) theoretically demonstrated that Trojans as massive as the main planet could be long-term stable, thus inspiring the concept of co-orbital planets. The fact that the stability condition for co-orbitals is met for pairs of bodies with similar masses opens the possibility of searching for exotrojans using the same methods and instruments as for the currently confirmed exoplanets (e.g., radial velocities, Giuppone et al. 2012, Leleu et al. 2015; transit timing variations, Haghighipour et al. 2013; transits themselves, Hippke & Angerhausen 2015; or the combination of transit and radial velocity data, Leleu et al. 2017). However, the efforts in the search for exotrojan planets have resulted in a select number of unconfirmed candidates so far (Lillo-Box et al. 2014, 2018a,b; Hippke & Angerhausen 2015).

Several numerical and hydrodynamical simulations on the evolution of planets embedded in protoplanetary disks agree in converging to solutions compatible with Trojan formation. These simulations show that dust particles preferentially accumulate at the L_4 and L_5 regions of the protoplanet (e.g., Laughlin & Chambers 2002; Beaugé et al. 2007; Montesinos et al. 2020). The enhanced dust growth at these locations can form planetesimals and, eventually, rocky bodies with masses as high as those of super-Earths (e.g., Lyra et al. 2009). Therefore, Trojans might be a natural byproduct of planetary formation through in situ formation mechanisms. Their assembling could be studied at the earliest stages, when protoplanets are still embedded within protoplanetary disks. Furthermore, they might be unique targets to study what protoplanet interiors are made of since Trojans and planets are most likely formed simultaneously (e.g., Bae et al. 2019 results suggest that grains have difficulties accumulating in the Lagrangian regions once the planet has carved a gap).

---

[1] The largest known is the Jupiter Trojan (624) Hektor, a bilobe-shaped body with an equivalent diameter of ∼220 km (Marchis et al. 2014).

High-angular resolution observations of protoplanetary disks (mainly in the submillimeter range) have shown that the presence of substructures such as gaps and rings is very common (e.g., Garufi et al. 2018; Andrews 2020; Benisty et al. 2022). In particular, two of those disks show continuum emissions that could be explained by dust accumulations in the Lagrangian regions of nondetected planets, thus becoming an indirect hint for the presence of such young protoplanets. One case is HD 163296, which shows a well-defined arc-like feature inside a gap satisfactorily reproduced by simulations of dust corotating with a potential protoplanet (Isella et al. 2018; Rodenkirch et al. 2021; Garrido-Deutelmoser et al. 2023). The other is LkCa 15, for which Long et al. 2022 have reported two emissions at ∼10-σ significance separated by 120° in azimuth with shapes comparable to those found in the simulations (e.g., Zhang et al. 2018). These claims are an indirect method to infer the presence of (as of yet undetected) protoplanets, and also the first piece of evidence of exotrojan formation.

The K7 T-Tauri star PDS 70 (Pecaut & Mamajek 2016; Müller et al. 2018) is a unique target for planetary formation studies since it harbors the only robust detection of two protoplanets. It is surrounded by a highly structured protoplanetary disk with a wide inner cavity presumably carved by the planets. Both planets have been observed at infrared and submillimeter wavelengths and at different epochs (e.g., Keppler et al. 2018; Wagner et al. 2018; Haffert et al. 2019; Isella et al. 2019; Benisty et al. 2021). This has enabled their orbits to be modeled and they appear to be migrating into a 2:1 mean motion resonance (Bae et al. 2019; Wang et al. 2021). As an example of how insightful this system is for planet formation studies, Benisty et al. 2021 recently reported the detection of emission colocated with PDS 70 c, which possibly is the first detection of a circumplanetary disk (CPD).

For this paper, through a reanalysis of archival public Atacama Large Millimeter/submillimeter Array (ALMA) data, we searched for excess emission compatible with dust accumulation in the Lagrangian regions of both protoplanets around PDS 70. This work is part of the TROY[2] project (Lillo-Box et al. 2018a), which is devoted to searching for the first exotrojans and studying their impact in planetary systems. In Sect. 2, we describe the observational data, and we present the results of our search in Sect. 3. Section 4 is dedicated to discussing a potential detection of dust accumulation in the L_5 region of PDS 70 b. We provide our conclusions in Sect. 5.

2. Observations

In this work, as a starting point, we use the combined self-calibrated ALMA dataset used by Benisty et al. (2021). They included submillimeter continuum data in Band 7 at wavelength 855 μm from program IDs 2018.A.00030.S, 2015.1.00888.S, and 2017.A.00006.S. In particular, we worked with their combination of three observations gathered at different epochs and different baselines. For more details on the calibration and the centering of these datasets, we refer the reader to the seminal publication.

The difference between the combined image shown in Benisty et al. (2021) and the one from this work is the imaging procedure. We used the Common Astronomy Software Applications package (CASA; McMullin et al. 2007) version 6.1.1. We imaged the visibilities of their self-calibrated data using the task `tclean`, a multifrequency synthesis mode, and a multiscale clean deconvolution algorithm with scales of 0, 1, and 2 times

the beam full width at half maximum. Briggs weighting (Briggs & Cornwell 1992) was tested using different robust parameters; finally, we chose $r = 1.7$ since it provided the best trade-off between sensitivity and angular resolution with the best signal-to-noise ratio (see Appendix A). A map size of 2000 × 2000 pixels was produced, with a pixel size of 0.005″. The final image was corrected from the primary beam response showing a synthesized beam size of 0.058″ × 0.052″, a position angle of 58.71°, and a root mean square (rms) equal to 11 μJy beam^{-1} calculated as the standard deviation in the whole image not corrected for the primary beam but excluding the disk. In order to follow a very conservative analysis of the data, we performed our analysis without applying the correction that was used in Benisty et al. (2021) to deal with a cleaning effect first described in Jorsater & van Moorsel (1995), the so-called JvM effect as the acronym of their names. Yet, we also show in Appendix A the impact of the robust parameter for JvM-corrected images. For an explanation of this correction, readers can refer to Appendix C and Czekala et al. (2021).

3. Results

The center of the combined ALMA image in the original publication (Benisty et al. 2021) is defined by the center of an ellipse fitting the emission maximum of the outer ring in the image plane. In order to avoid any effect induced by different cleaning processes, we centered the orbit using as a criterion that the reported position by the authors of planet c must match the maximum of its submillimeter emission. This corresponds with an offset with respect to the center of the observations of ΔRA = 9.5 mas and ΔDec = 12.5 mas (center marked with white lines in Fig. 1), which is compatible with their uncertainties and also is in good agreement with the offset reported by the authors when modeling the outer disk with the `frank` (Jennings et al. 2020) package (ΔRA = 12 mas and ΔDec = 15 mas).

We projected the orbits of PDS 70 b and c onto the image based on the orbital parameters derived by Wang et al. (2021). We generated 10^3 random orbits for each planet taking normal distributions centered in the dynamically stable parameters within 1-σ (see Table 3 from their work). Additionally, we restricted the orbits to those that cross the positions of the submillimeter peak emissions associated with both planets in our image (as reported by Benisty et al. 2021). For each of the orbits, we located the corresponding minimum of the gravitational well of the L_4 and L_5 points, at ±60° in azimuth from those peak intensities within the orbits. In Fig. 1 we show the PDS 70 continuum image with the contour lines corresponding to 3, 3.5, 4, and 8-σ, where σ is the rms of the image as stated in Sect. 2. Table B.1 lists the positions for the maximum of the submillimeter emission associated with the planets and their Lagrangian points at the time of the long baseline observations (July 2019).

From Fig. 1, we visually find a match between a submillimeter unresolved compact emission detected with a significance of near 4-σ (∼6-σ with the JvM-corrected image, see Appendix C) and the expected position of the L_5 point of the submillimeter extended emission associated with PDS 70 b (hereafter L_{5b}[3]). Conversely to planet c, the peak of the submillimeter emission associated with PDS 70 b is shifted from the infrared centroid as already discussed by Isella et al. (2019) and Benisty et al. (2021). In Appendix D, we show the same exercise but considering the infrared position of the planet, concluding that this new compact

---

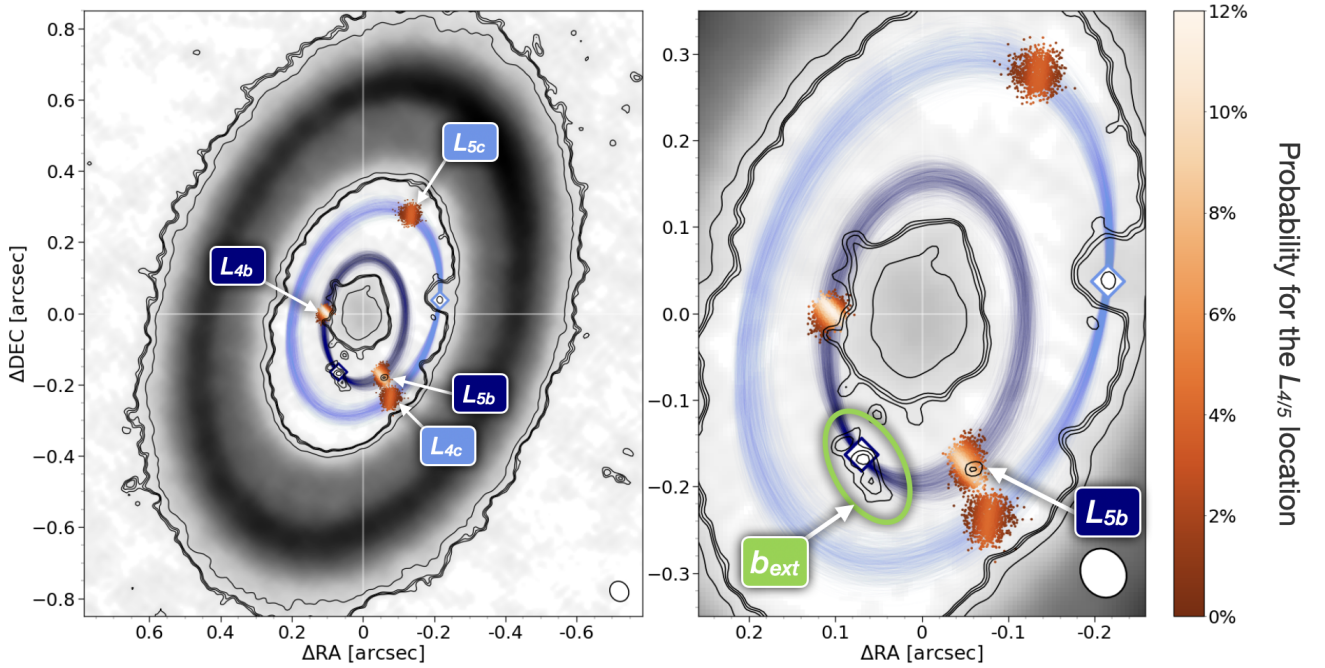3 We use equivalent notation for the other Lagrangian regions.

Fig. 1. PDS 70 ALMA observations with the projected distributions of the projected planetary orbits and Lagrangian points (L_4 and L_5) distributions. The background image (inverted grayscale) corresponds to the continuum observations from the combined ALMA data (see Sect. 2). The locations for the corresponding L_4/L_5 points for each orbit (total of 10^3 for each planet) are plotted with dots, whose density is represented by the colors from the right-hand side bar (it is important to note that lighter colors denote a higher density of probability for the location). The origin of coordinates is shown with white lines. The synthesized beam ($0.058'' \times 0.052''$, PA = $58.71°$) is represented in the bottom right of each panel by a white ellipse. Diamond-shaped markers indicate the planets locations. Contours correspond to 3, 3.5, 4, and 8-σ. *Left*: global picture of PDS 70. *Right*: zoom of the inner cavity to inspect the L_5 region of PDS 70 b. In green the extended emission associated with planet b reported by Isella et al. 2019 is indicated.

emission is fully compatible with dust librating within the L_{5b} region.

We found this new emission using the same dataset published in Benisty et al. (2021) as the result of carrying out a cleaning focused on maximizing the signal-to-noise ratio within the disk cavity. Their goal was the analysis of the CPD around PDS 70 c whose emission is noticeably stronger and thus they did not require a cleaning so close to the noise level. To reach the required sensitivity for this tentative detection, it has been key to use the combined data from the three different epochs. We have checked that over these epochs no effect is expected due to the motion of the emission in L_{5b}. Between August 2016 and July 2019, the motion following the orbit of planet b should have been around half of the beam size, and thus not being sensitive to it.

We can carry out a rough estimation of the dust mass potentially trapped in the L_{5b} region by using the equation derived by Hildebrand (1983), for which the dust mass (M_d) scales with the flux density (F_ν):

$$M_d = \frac{F_\nu d^2}{\kappa_\nu B_\nu(T)}, \tag{1}$$

where d is the distance to the source, κ_ν the dust opacity, and $B_\nu(T)$ the blackbody emission for a source with an effective temperature T. We assume that the emission at 855 μm is optically thin and that it comes from dust thermal emission. The estimated flux density of the compact emission, which is the same as the peak intensity for an unresolved source, is 40 μJy. We assume a dust temperature of 19 K as estimated by Keppler et al. (2019) due to the stellar irradiation at the separation of PDS 70 b ($\sim$22 au), and we used the dust opacity from Birnstiel et al. (2018) at a close frequency as an approximation

($\kappa_{0.88\,mm} = 3.6\,cm^2\,g^{-1}$). We consider an uncertainty in the temperature of ±5 K, a 25% in the dust opacity, and $\sqrt{rms^2 + \Delta F_{calib}^2}$ for the density flux, where we took $\Delta F_{calib} = 10\%$ of the measured density flux. Thus, the dust mass traced at this wavelength is in the range of $0.0004-0.02\,M_\oplus$, or equivalently $0.03-2\,M_{Moon}$.

4. Discussion

Detecting the co-orbital motion of both the planet and the L_{5b} emission along the expected orbital path would provide additional evidence in favor of the exotrojan dust scenario. We consider a minimum spatial separation equal to the synthesized beam to be able to detect motions of planets and Trojans between two epochs, considering that the size of the synthesized beam is larger than the absolute astrometric accuracy, which in a very unfavorable scenario of poor atmospheric phase stability could be $\sim 0.02''$ for a 4-σ detection. Assuming that additional data of a similar quality (at least the same sensitivity and spatial resolution) are obtained in the near future, we studied the epoch when the orbital motion will be enough to move to a projected distance equivalent to the beam size. In Table B.1 and Fig. 2, the July 2019 positions of the planets and their Lagrangian regions with their expected locations in February 2026 and November 2028 are compared. In the case of PDS 70 b, it will have moved a projected distance of $0.065''$ by February 2026. This is the earliest that we will be able to detect the motion of the three relevant locations of the orbit (planet b, L_{4b}, and L_{5b}). This date is 6.6 years after the epoch of the ALMA image used in this work, which is $\sim$6% of its orbital period ($P_b = 113 \pm 19$ yr). This
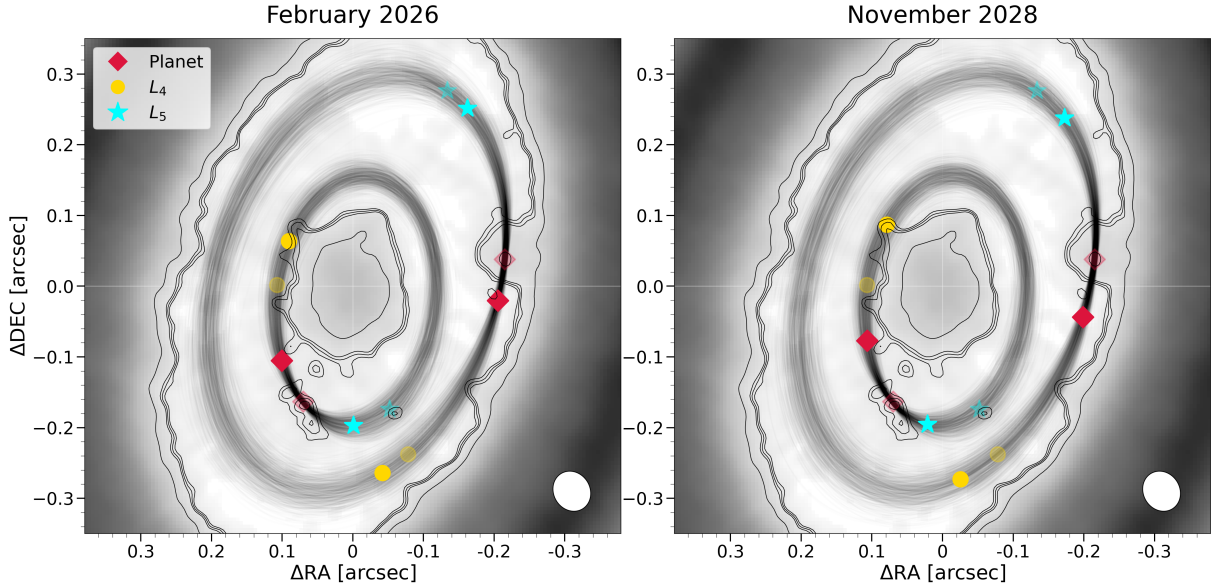
Fig. 2. Prediction for the positions of the planets and their Lagrangian points at different epochs. *Left*: minimum observing date to detect the co-orbital motion in the orbit of planet PDS 70 b. *Right*: equivalent for the orbit of planet PDS 70 c. Transparent symbols are the position in the current image epoch (July 2019), while solid symbols are for the epoch in the title. Same ALMA continuum image with the same projected orbits as in Fig. 1. Contours are 3, 3.5, 4, and 8-σ.

would be possible from Cycle 12 onward due to spatial resolution considerations following the ALMA observatory long-term configuration schedule[4].

We warn that this exercise is most favorable when performed at similar frequencies (i.e., Band 7). Dust grains with different sizes have different degrees of coupling to the gas and thus different dynamics (e.g., Lyra et al. 2009; Montesinos et al. 2020), and the extension and center of the emission may change. Indeed, this could explain the shift in the putative Trojan emissions detected in LkCa 15 when comparing Band 6 and 7 data by Long et al. (2022). Hence, to study the future orbital motion of the reported dust emission, it is better to perform observations at similar frequencies to guarantee that we are tracing the same dust population. If the Trojan nature of the L_{5b} emission is confirmed, observations at different frequencies could provide complementary information, which would be valuable to understand the evolution of different dust grain-size populations in the co-orbital regions. These data would be very helpful to test different model predictions investigating the dust population at the two Lagrangian regions. For instance, two independent authors (Montesinos et al. 2020; Rodenkirch et al. 2021) predict that the L_4 region tends to harbor smaller dust grains than L_5.

Seminal works using these data speculate on the unclear nature of the extended emission associated with planet b (shown in green in the right panel of Fig. 1). Isella et al. (2019) propose different scenarios: circumplanetary dust, a trace of dust particles trapped in L_5, or a jet similar to those detected in accreting protostars. In this work, we identify an additional emission spatially compatible with the potential gravitational well of L_{5b}. Hence, it may support the trace of dust from the trailing Lagrangian point hypothesis. In particular, a plausible explanation for this extended emission could be that planet b dominates over the gravity of the forming Trojan and, therefore, it can be stealing the material from the surroundings leading to the starvation of its companion (e.g., Cresswell & Nelson 2009 argue

that gas accretion increases the mass difference between the co-orbital pair).

It is important to highlight that co-orbital motion does not necessarily mean that the material is orbiting in the surroundings of the minimum of the gravitational wells of the Lagrangian points L_4/L_5. Indeed, the libration amplitude can even enclose both of these points as well as L_3 at the same time, what is known as a horseshoe orbit. For this reason, other substructures that are in the orbital path of the planets but do not exactly fall at the minimum of the gravitational wells could also be dust trapped in corotation. In the case of planet b, some substructures are seen coming out from the inner disk and near the location of L_{4b}. Nonetheless, this region is so close to the inner disk that it prevents us from reaching any conclusion about its nature. Similarly, halfway between planet c and L_{4c} there is a prominence in the inner edge of the outer disk that falls in the orbital path of the outer planet. Higher angular resolution observations would be required to test if this emission could be separated from the outer disk and whether it moves in corotation with PDS 70 c. The fact that the most convincing of the signatures compatible with co-orbital dust is at the L_5 region rather than L_4 might be consistent with the theoretical results found in previous works. For instance, Montesinos et al. (2020) point out that planets create an overdensity in L_5 compared to L_4 that results in an asymmetry in the total bulk mass which is always in favor of the trailing Lagrangian region, and thus it is expected that more massive bodies will be found there than in the leading region.

5. Conclusions

We reanalyzed the combined ALMA observations of PDS 70 presented in Benisty et al. (2021) by performing an independent cleaning to search for dust accumulation in the Lagrangian regions of the two detected protoplanets. We find tentative emission at ∼4-σ significance at the expected position of the Lagrangian region L_5 of planet PDS 70 b, which is thus a candidate precursor for the formation of a co-orbital body, or even the leftovers of a massive Trojan body that has already formed. This would be the third claim of dust trapping in a Lagrangian

---

[4] https://almascience.nrao.edu/observing/observing-configuration-schedule/long-term-configuration-schedule

region of a protoplanet (the former ones were in HD 163296 and LkCa 15 disks). Nonetheless, this is the first time the position of such emission can be associated with the expected location of the Lagrangian region of a confirmed planet. For the sake of confirming or rejecting the Trojan candidate, we propose that future ALMA observations revisit the system. Since the orbit of PDS 70 b is known, we have shown that beyond 2026 we may be able to resolve the co-orbital motion.

If confirmed, this work represents observational support to the hypothesis of Trojan bodies being a common consequence of planetary formation. It encourages further surveys to find them in both young and evolved systems. Their existence and properties (chemical and dynamical) would provide additional hints for understanding the evolution of planetary systems as a whole. On the other hand, although ALMA is currently making such discoveries possible, its planed wideband sensitivity upgrade (the top priority initiative for the ALMA2030 Development Roadmap) will be crucial to perform these studies in a much more efficient way.

References

Andrews, S. M. 2020, ARA&A, 58, 483
Bae, J., Zhu, Z., Baruteau, C., et al. 2019, ApJ, 884, L41
Beaugé, C., Sándor, Z., Érdi, B., & Süli, Á. 2007, A&A, 463, 359
Benisty, M., Bae, J., Facchini, S., et al. 2021, ApJ, 916, L2
Benisty, M., Dominik, C., Follette, K., et al. 2022, ArXiv e-prints [arXiv:2203.09991]
Birnstiel, T., Dullemond, C. P., Zhu, Z., et al. 2018, ApJ, 869, L45
Briggs, D. S., & Cornwell, T. J. 1992, in Astronomical Society of the Pacific Conference Series, 25, Astronomical Data Analysis Software and Systems I, ed. D. M. Worrall, C. Biemesderfer, & J. Barnes, 170
Cresswell, P., & Nelson, R. P. 2009, A&A, 493, 1141
Czekala, I., Loomis, R. A., Teague, R., et al. 2021, ApJS, 257, 2
Garrido-Deutelmoser, J., Petrovich, C., Charalambous, C., Gúzman, V. V., & Zhang, K. 2023, ApJ, 945, L37
Garufi, A., Benisty, M., Pinilla, P., et al. 2018, A&A, 620, A94
Giuppone, C. A., Benítez-Llambay, P., & Beaugé, C. 2012, MNRAS, 421, 356
Haffert, S. Y., Bohn, A. J., de Boer, J., et al. 2019, Nat. Astron., 3, 749
Haghighipour, N., Capen, S., & Hinse, T. C. 2013, Celest. Mech. Dyn. Astron., 117, 75
Hildebrand, R. H. 1983, QJRAS, 24, 267
Hippke, M., & Angerhausen, D. 2015, ApJ, 811, 1
Isella, A., Huang, J., Andrews, S. M., et al. 2018, ApJ, 869, L49
Isella, A., Benisty, M., Teague, R., et al. 2019, ApJ, 879, L25
Jennings, J., Booth, R. A., Tazzari, M., Rosotti, G. P., & Clarke, C. J. 2020, MNRAS, 495, 3209
Jorsater, S., & van Moorsel, G. A. 1995, AJ, 110, 2037
Keppler, M., Benisty, M., Müller, A., et al. 2018, A&A, 617, A44
Keppler, M., Teague, R., Bae, J., et al. 2019, A&A, 625, A118
Laughlin, G., & Chambers, J. E. 2002, AJ, 124, 592
Leleu, A., Robutel, P., & Correia, A. C. M. 2015, A&A, 581, A128
Leleu, A., Robutel, P., Correia, A. C. M., & Lillo-Box, J. 2017, A&A, 599, A7
Lillo-Box, J., Barrado, D., Moya, A., et al. 2014, A&A, 562, A109
Lillo-Box, J., Barrado, D., Figueira, P., et al. 2018a, A&A, 609, A96
Lillo-Box, J., Leleu, A., Parviainen, H., et al. 2018b, A&A, 618, A42
Long, F., Andrews, S. M., Zhang, S., et al. 2022, ApJ, 937, L1
Lyra, W., Johansen, A., Klahr, H., & Piskunov, N. 2009, A&A, 493, 1125
Marchis, F., Durech, J., Castillo-Rogez, J., et al. 2014, ApJ, 783, L37
McMullin, J. P., Waters, B., Schiebel, D., Young, W., & Golap, K. 2007, in Astronomical Society of the Pacific Conference Series, 376, Astronomical Data Analysis Software and Systems XVI, eds. R. A. Shaw, F. Hill, & D. J. Bell, 127
Montesinos, M., Garrido-Deutelmoser, J., Olofsson, J., et al. 2020, A&A, 642, A224
Müller, A., Keppler, M., Henning, T., et al. 2018, A&A, 617, A2
Pecaut, M. J., & Mamajek, E. E. 2016, MNRAS, 461, 794
Rodenkirch, P. J., Rometsch, T., Dullemond, C. P., Weber, P., & Kley, W. 2021, A&A, 647, A174
Wagner, K., Follete, K. B., Close, L. M., et al. 2018, ApJ, 863, L8
Wang, J. J., Vigan, A., Lacour, S., et al. 2021, AJ, 161, 148
Zhang, S., Zhu, Z., Huang, J., et al. 2018, ApJ, 869, L47

Appendix A: Gallery of images for different Briggs robust values

In Fig. A.1 we show a gallery of images changing the Briggs robust parameter in the CASA cleaning routine. In all of them, the emission at L_{5b} is found with a significance between 3 and 4-σ, increasing for higher robust parameters since the sensitivity improves. The image shown in this work (see Fig. 1) uses r = 1.7. This is the value that maximizes the signal-to-noise ratio for our image in the inner cavity and hence provides the highest significance for the tentative detection. In Table A.1 we summarize the beam, rms, peak intensity, and significance of the emission for each of those images.

Table A.1. Properties for the images with different robust values shown in Fig. A.1.

JvM corrected	Briggs Parameter	Beam [mas × mas, °]	rms [μJy beam^{-1}]	Peak intensity L_{5b} [μJy beam^{-1}]	Significance L_{5b} emission
No	-0.5	21 × 21, 29.66	25.2	79.0	3.1-σ
	0.0	28 × 25, 40.96	17.3	56.4	3.3-σ
	0.5	44 × 36, 51.78	12.7	41.4	3.3-σ
	1.0	54 × 47, 57.33	11.3	38.3	3.4-σ
	1.5	58 × 51, 58.60	10.9	39.6	3.6-σ
	1.7	58 × 56, 58.71	10.9	39.9	3.7-σ
	2.0	59 × 52, 58.77	10.9	38.4	3.5-σ
Yes	-0.5	21 × 21, 29.66	18.9	59.3	3.1-σ
	0.0	28 × 25, 40.96	11.3	36.7	3.3-σ
	0.5	44 × 36, 51.78	7.36	25.4	3.4-σ
	1.0	54 × 47, 57.33	3.77	16.7	3.4-σ
	1.5	58 × 51, 58.60	3.08	18.0	5.8-σ
	1.7	58 × 56, 58.71	3.22	18.5	5.7-σ
	2.0	59 × 52, 58.77	3.01	14.9	5.0-σ

Appendix B: Predicted astrometry to detect the co-orbital motion

Table B.1. Coordinates with respect to the center of our image for the peak submillimeter emission of PDS 70 b and c and their L_4 and L_5 Lagrangian points. July 2019 is the epoch of the long baseline observation used in the composed image of this work. February 2026 and November 2028 are the minimum predicted dates to measure the co-orbital motion in PDS 70 b and c orbits, respectively.

	July 2019		February 2026		November 2028	
	ΔRA [mas]	ΔDEC [mas]	ΔRA [mas]	ΔDEC [mas]	ΔRA [mas]	ΔDEC [mas]
PDS 70 b	70.1 ± 2.5	− 163.0 ± 3.4	100.3 ± 5.0	− 105.4 ± 7.0	106.5 ± 6.0	− 77 ± 11
L_{4b}	107.0 ± 9.0	2.8 ± 9.0	90 ± 10	63 ± 10	79 ± 11	87 ± 10
L_{5b}	− 51.8 ± 9.0	− 174 ± 15	− 0.9 ± 5.0	− 196 ± 11	21.4 ± 8.0	− 194.5 ± 9.0
PDS 70 c	− 215.1 ± 1.8	37.8 ± 3.7	− 205.2 ± 4.0	− 19.9 ± 5.0	− 199.0 ± 5.0	− 43.7 ± 6.0
L_{4c}	− 77 ± 13	− 238 ± 14	− 42 ± 12	− 264 ± 13	− 25 ± 15	− 273 ± 15
L_{5c}	− 134 ± 13	275 ± 13	− 162 ± 10	251 ± 14	− 173 ± 11	237 ± 12

Appendix C: JvM-corrected image

In the cleaning process, the final image is the result of combining the model and the residual images. Nonetheless, there is a mismatch between the units of both images (Jy/CLEAN beam and Jy/dirty beam, respectively). Thus, the resulting flux scale is incorrect (Jorsater & van Moorsel 1995). Following the methodology of Czekala et al. (2021), we corrected for this JvM effect by rescaling the residual image by the CLEAN beam/dirty beam volumes ratio before combining it with the model. We show the cleaned image in Fig. C.1. In particular, the emission falling in our interest region L_{5b} turns out to be at a 5.7-σ level since the rms when using this correction is 3.2 μJy beam^{-1} and the peak intensity is 18.5 μJy beam^{-1}.
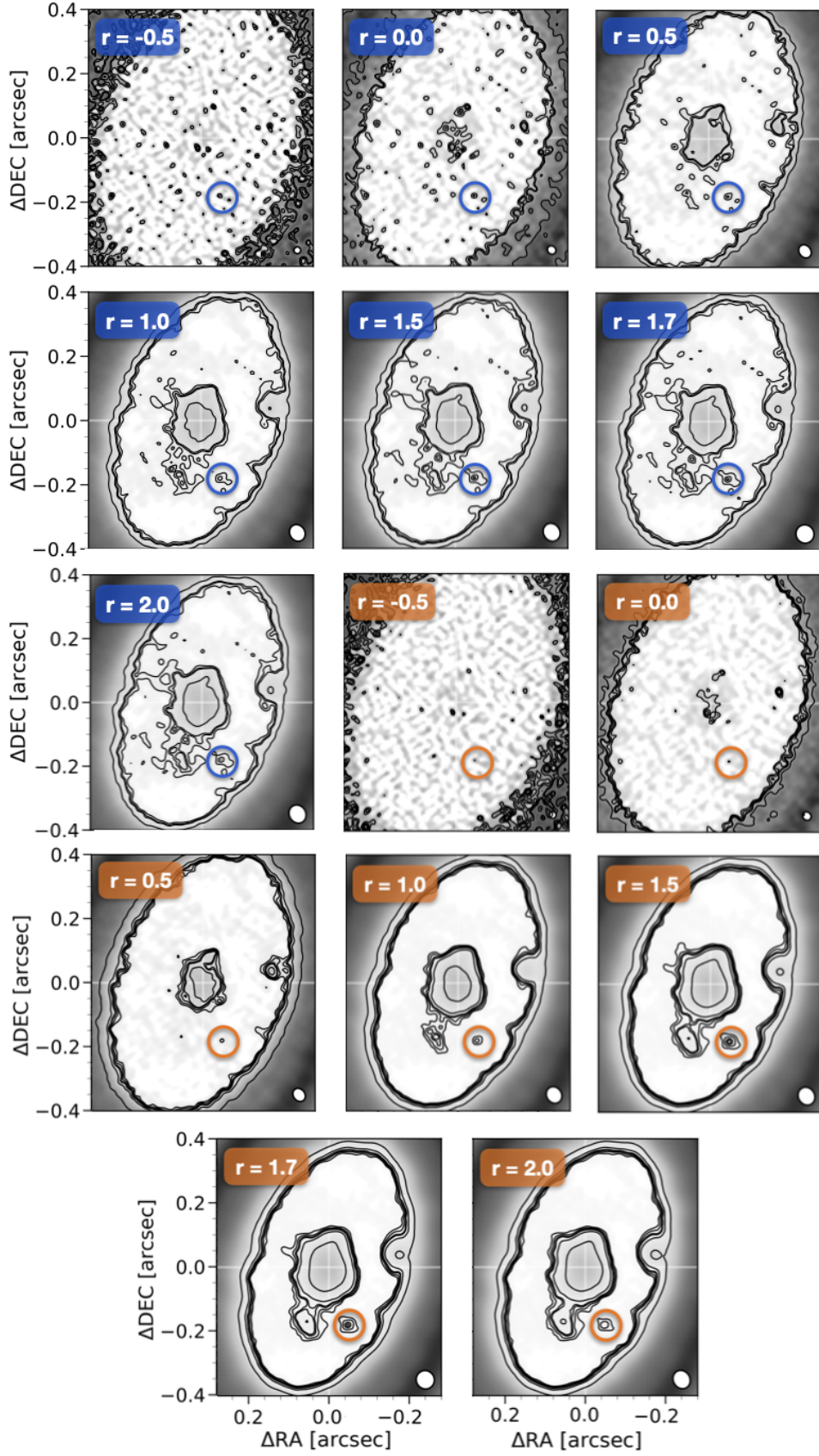
Fig. A.1. Gallery of images with different robust values as indicated in the upper left corner of each panel. The circle indicates the position of the L_{5b} emission. Panels with blue colors correspond with the image without the JvM correction, whose contours are 2, 3, 3.5, and 8-σ. Panels with orange colors are JvM-corrected images and their contours indicate 3, 4, 5, 5.5, 8, and 22-σ.
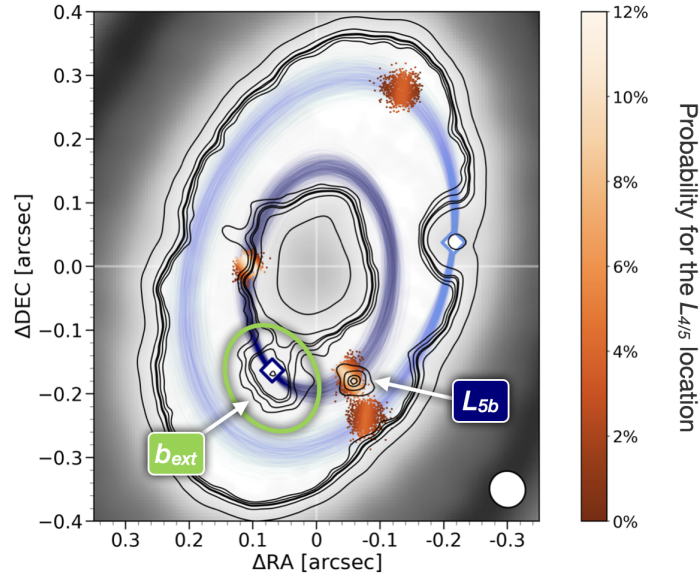
Fig. C.1. Same image as in Fig. 1, but applying the JvM correction. Contours are 3, 4, 5, 5.5, 8, and 22-σ. The L_{5b} submillimeter emission here is detected at ~6-σ of significance.

Appendix D: Shift between submillimeter and infrared emission of PDS 70 b

In order to consider the reported shift between the infrared and submillimeter positions for planet b, we derived the location of the L_5 point associated with the infrared position of the planet. We used the position inferred in Wang et al. (2021) from the GRAVITY observations in the K band, taken at the same epoch as the ALMA long baseline observations (July 2019): ΔRA = (102.61 ± 0.09) mas and ΔDEC = (-139.93 ± 0.24) mas. In Fig. D.1 we compare the orbits of planet b when restricting them to the location of the planet in the infrared (red), and to the maximum of the submillimeter emission as in the main text (blue). The locations of the L_5 points for each case are indicated with solid circles. As discussed in the main text, the blue circle perfectly matches the compact emission tentatively detected, while it is ~5° in azimuth backward of the L_5 point associated with the PDS 70 b infrared position. The orbital paths in both cases (blue and red) cross the detected emission. Hence, this compact emission perfectly lies within the Lagrangian region of the planet, and it might be dust trapped in its potential well, co-orbiting with PDS 70 b and librating in its L_5 point.
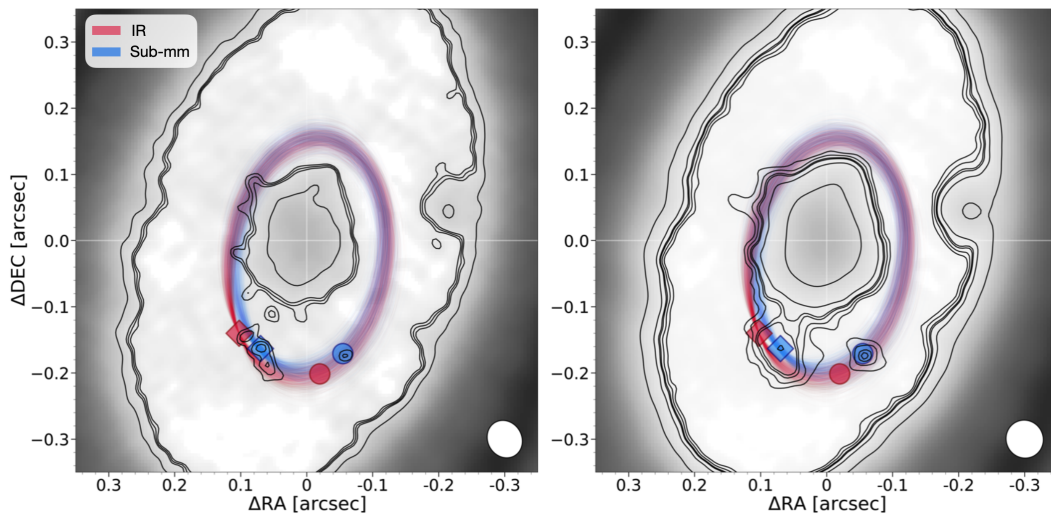

Fig. D.1. Same ALMA image and contours as in Fig. 1 (*left*) and Fig. C.1 (*right*, which is JvM corrected), but including the infrared position of planet PDS 70 b. Diamond markers indicate the infrared position of PDS 70 b (in red) and the maximum of the submillimeter emission associated with PDS 70 b (in blue). The orbits are restricted to those crossing the position of the markers in each case. The big solid circles represent the location of the L_5 points associated with the infrared position of the planet (in red) and with the peak of the submillimeter emission (in blue), respectively.